Journal of Alloys and Compounds 689 (2016) 1044–1050

Contents lists available at ScienceDirect

Journal of Alloys and Compounds

journal homepage: http://www.elsevier.com/locate/jalcom

Multivariable tuning of the magnetostructural response of a Ni-modified FeRh compound

R. Barua [a, b, *], I. McDonald [a], F. Jiménez-Villacorta [a, 1], D. Heiman [c], L.H. Lewis [a, b, d]

[a] Department of Chemical Engineering, Northeastern University, Boston, MA 02115, USA
[b] George J. Kostas Research Institute for Homeland Security, Northeastern University, Burlington, MA, USA
[c] Department of Physics, Northeastern University, Boston, MA 02115, USA
[d] Dept. of Mechanical and Industrial Engineering, Northeastern University, Boston, MA 02115, USA

ARTICLE INFO

Article history:
Received 1 April 2016
Received in revised form
22 June 2016
Accepted 1 August 2016
Available online 3 August 2016

Keywords:
Magnetostructural response
Magnetocaloric response
FeRh

ABSTRACT

The magnetostructural response of a Ni-modified B2-type FeRh compound of composition, $(Fe_{47.5}Ni_{1.5})Rh_{51}$, is reported under the influence of simultaneous variations in temperature, applied magnetic field and hydrostatic pressure. The material undergoes a first-order magnetic transition from the antiferromagnetic state to the ferromagnetic state at a reduced temperature $T_t = 144$ K in the absence of applied magnetic field $\mu_0 H$ and applied pressure P. Applied independently, pressure and magnetic field influence T_t in opposite ways, with $[dT_t/dH]_{P=0} = -24\ K/T$ and $[dT_t/dP]_{H=0} = 15\ K/kbar$, which are 3 time larger than in the parent compound FeRh. Application of Maxwell's relations to the magnetization data allows determination of the entropy change of the compound, and thus evaluates its magnetocaloric potential through the transition. Pressure application increases the magnetic entropy change (ΔS_{mag}) but decreases the width of the magnetostructural transition, thereby decreasing the refrigeration capacity. Application of pressure also drives the phase transition to lower temperatures; it becomes sluggish and eventually is completely arrested below a critical temperature of ~75 K. A three-dimensional ($\mu_0 H$–P–T) phase diagram is constructed for the magnetic transition in the $(Fe_{47.5}Ni_{1.5})Rh_{51}$ system in order to evaluate the isocompositional magnetostructural response to combined application of pressure and magnetic field. Overall, these results emphasize that the magnetostructural phenomena in FeRh-based compounds is a thermally-activated process that may be tuned predictably by a variety of intrinsic (elemental substitution) and extrinsic (pressure, magnetic field, temperature) factors.

1. Introduction

Magnetic materials that undergo magnetostructural phase transitions typically exhibit simultaneous magnetic and structural phase changes of an abrupt and hysteretic nature as a result of strong lattice-spin coupling. In the vicinity of the magnetostructural transition, select materials systems exhibit exceptional functional effects (examples: giant magnetostrictive and giant magnetoresistive effects) in response to small changes in an intensive thermodynamic variable such as temperature T, pressure P or applied magnetic field $\mu_0 H_{app}$ [1–6]. These effects lend magnetostructural materials diverse functionality suitable for use in potential technological applications including thermal sensors [7], magnetic refrigeration devices [8], energy-harvesting converters [9] and data storage systems [10,11]. In this study, the B2-ordered (CsCl type) α''-phase of $Fe_{1-x}Rh_x$ ($0.46 < x < 0.52$) serves as a test bed for advancing understanding of fundamental spin-lattice interactions in intermetallic compounds that exhibit the magnetostructural phase transformation phenomena.

In bulk form, equiatomic FeRh exhibits an abrupt antiferromagnetic (AFM) to ferromagnetic (FM) transition upon heating to a transition temperature of T_t ~ 350 K, typically with a 10° thermal hysteresis between the heating and cooling cycles [12]. The thermodynamically first-order AFM → FM magnetic phase transition in FeRh is accompanied by a 1% unit cell volume expansion without change in crystal symmetry [13], a large change in magnetic entropy ($\Delta S_{mag} = 12.58$ J/kg K) [14] and a significant evolution of latent heat ($\Delta H = 5.1$ J/g) [15]. Outstanding caloric effects upon

* Corresponding author. Department of Chemical Engineering, Northeastern University, Boston, MA 02115, USA.
E-mail addresses: radhika.barua@gmail.com, r.barua@neu.edu (R. Barua).
[1] Current address: Materials Science Institute of Madrid (ICMM-CSIC), C/ Sor Juana Inés de la Cruz, 3. 28049 Madrid, Spain.

http://dx.doi.org/10.1016/j.jallcom.2016.08.004
0925-8388/

application and removal of a magnetic field are reported for this compound including a giant magnetocaloric effect ($\Delta T = 12.9$ K at $\mu_0 H_{app} = 2$ T [17]), a giant elastocaloric effect ($\Delta T = 5.17$ K at a tensile stress of 529 MN/m^2 [4]) and a giant barocaloric effect ($\Delta S/\Delta P = 12$ J kg^{-1}K^{-1}kbar^{-1} [3]). Numerous theoretical and experimental studies indicate that the magnetostructural response and associated caloric effects in FeRh can be driven via a variety of extrinsic parameters, namely temperature, pressure and magnetic field [16–24]. In particular, the transition temperature T_t of equiatomic FeRh increases with increased hydrostatic pressure at zero applied magnetic field ($[\partial T_t/\partial P]_{H=0} = 5 \times 10^{-3}$ K/atm) [17,19,20] and decreases with increased magnetic field at zero applied pressure ($[\partial T_t/\partial H]_{P=0} = 8$ K/T) [14,17]. To date, the influence of the simultaneous application of two or more extrinsic parameters on the magnetostructural response of FeRh-based compounds remains unclear. This current work seeks to address this knowledge gap.

Early work conducted by Wayne in 1968 addresses the dependence of pressure and magnetic field on the magnetostructural response of a series of FeRh-based ternary compounds within the framework of Maxwell's relations of thermodynamics [17]. Wayne's work was instrumental in demonstrating that Kittel's exchange inversion theory, which proposes that the exchange interaction integral (J_{ex}) between the Fe-Fe atoms in the FeRh lattice depends linearly on the lattice parameter and changes sign at a certain critical value of that parameter [12], is not an acceptable model to explain the magnetostructural behavior of FeRh. Further, Wayne observed that the ratio of $\partial T_t/\partial H$ and $\partial T_t/\partial P$ in a variety of FeRh-based ternary compounds is almost constant at $\frac{\partial T_t}{\partial H}/\frac{\partial T_t}{\partial P} \sim 1.73$ *kbar*/*T* [17]. Building on Wayne's results, Kushwaha *et al.* more recently constructed empirical curves ($\frac{\partial T_t}{\partial H}$ and $\frac{\partial T_t}{\partial H}$) to predict the pressure and magnetic field dependence of the magnetostructural response of a variety of transition-metal-doped FeRh compounds [24]. Kushwaha *et al.* utilized resistivity data to scrutinize the magnetostructural behavior of select Pd-doped FeRh compounds under simultaneous application of magnetic field (up to 8 T) and pressure (up to 20 kbar) [25]. Overall, Kushwaha *et al.* found that the kinetics of the phase transformation phenomena in $Fe_{48}(Rh_{0.93}Pd_{0.07})_{51}$, as indicated by the extent of thermal hysteresis in the magnetization data, depends very little on the magnitude of applied pressure and magnetic field [24,25].

In this current work, a Ni-modified alloy of nominal composition $(Fe_{47.5}Ni_{1.5})Rh_{51}$ is employed as a model system to quantify the effects of simultaneous application of temperature *T*, magnetic field $\mu_0 H$ and pressure *P* on the magnetostructural response of FeRh-based systems. At zero applied pressure and zero applied magnetic field the $(Fe_{47.5}Ni_{1.5})Rh_{51}$ composition demonstrates a first-order magnetostructural phase transition at ~150 K, allowing it to be readily probed with laboratory-based equipment. Results obtained in this work shed light on key aspects of the magnetostructural phase transformation process in chemically-ordered FeRh compounds and indicate that magnetostructural phenomena is a thermally-activated process that is driven by both the electronic structure of the system and by a magnetovolume effect. This study also provides the first report of the effect of hydrostatic pressure on the magnetocaloric response of a Ni-doped B2-type FeRh compound. It is anticipated that the data and associated trends reported here can serve as guidelines for tailoring magnetostructural transitions in related caloric compounds for emerging technological applications.

2. Experimental methods

A Ni-substituted FeRh-based sample of composition $(Fe_{47.5}Ni_{1.5})Rh_{51}$ was synthesized by arc melting the constituent elements (99.9% purity) in an Ar atmosphere. The arc-melted ingot was sealed under vacuum (1×10^{-6} Torr) in vitreous silica tubes and annealed at 1000 °C for 48 h to develop the chemically-ordered B2 CsCl-type structure. The chemical composition and homogeneity of the sample were confirmed by scanning electron microscopy (SEM) energy-dispersive X-ray spectroscopy (EDS) (Hitachi S4800) and attainment of the B2-ordered crystal structure was verified using X-ray diffraction (XRD; PANanalytical X'Pert PRO**).** Lattice parameters were obtained using a least squares procedure [26] and the chemical order parameter *S* was determined as

$$S = \sqrt{I_{001}^{\exp}/I_{002}^{\exp}} \Big/ \sqrt{I_{001}^{calc}/I_{002}^{calc}} \tag{1}$$

where I_{001}^{exp} and I_{001}^{calc} are the experimental and theoretical intensities of the (00l) B2 superlattice Bragg reflections and I_{002}^{exp} and I_{002}^{calc} are the experimental and theoretical intensities of the fundamental (002) Bragg reflections.

Magnetization measurements carried out at ambient and hydrostatic pressures (0 kbar $\leq P <$ 10 kbar) were performed using SQUID magnetometry in fields up to 5 T and in the temperature range 2 K < T < 325 K. Hydrostatic pressure was applied to the sample using a CuBe piston clamp pressure cell (Mcell 10 manufactured by Almax EasyLab [27]). To minimize errors due to differential thermal contraction between the metallic components of the pressure cell and the pressure transmitting medium, the temperature sweep-rate during measurement was set at 1 K/min. The pressure inside the cell was calibrated *in situ* by measurement of the shift of the superconducting transition temperature of a sample of tin (Sn). The thermomagnetic behavior of the $(Fe_{47.5}Ni_{1.5})Rh_{51}$ sample was studied under both zero-field-cooled (ZFC) and field-cooled (FC) conditions. During the ZFC measurement mode, the sample was initially cooled to 50 K under zero applied magnetic field and data were collected upon increasing temperature in an applied field range 0.5 T < $\mu_0 H_{app}$ < 5 T. In the FC measurement mode, the data were collected while cooling and heating the sample at the same applied magnetic field as was used in the ZFC experiment. The magnetostructural phase transition temperature was determined as the maximum of the derivative of magnetization *M* with respect to *T* (*i.e.* $(dM/dT)_{max}$) and the width of the thermal hysteresis (ΔT_t) of the phase transition was determined as the difference between the transition temperatures obtained upon heating through the AF→FM transition (T_t^{hc}) and cooling through the FM→AF transition (T_t^{cc}).

The magnetic entropy change (ΔS_{mag}) was determined from the Maxwell relation employing isothermal *M*(*H*) curves measured at temperature intervals of 2.5 K in the vicinity of the magnetostructural transition temperature [10] using Eq. (2):

$$\Delta S_{mag}\left(\frac{T_1 - T_2}{2}\right) = \frac{1}{T_1 - T_2}\left[\int_0^{H_{max}} M(T_2, H)\mathrm{d}H - \int_0^{H_{max}} M(T_1, H)\mathrm{d}H\right] \tag{2}$$

Here, T_1 and T_2 are two arbitrary temperatures near T_t. The area encompassed by the two *M*-*H* curves obtained at temperatures T_1 and T_2 is divided by the temperature difference, $\Delta T = T_2 - T_1$ to determine the magnetic entropy change ΔS_{mag} at an average temperature $T = (T_2 + T_1)/2$. To ensure reproducibility of results, prior to measurement of each *M*(*H*) curve the magnetic history of the sample was reset by cooling the sample down to the antiferromagnetic temperature range ($T = 50$ K). As per the protocol articulated by Manekar *et al.* [28], the magnetic entropy change ΔS_{mag} of

the sample was calculated using the second magnetization cycle rather than the initial magnetization curve. From an applications standpoint, a useful parameter to evaluate the magnetocaloric behavior of a materials system is the refrigeration capacity (*RC*) that quantifies the amount of heat that can be transferred during one magnetic refrigeration cycle [5]. To this end, the *RC* of $(Fe_{47.5}Ni_{1.5})Rh_{51}$ was estimated from the magnetic entropy curves (ΔS_{mag} *vs.* *T*) of the sample using Eq. (3):

$$RC(H_{app}) = \int_{T_{cold}}^{T_{hot}} \Delta S_{mag}(T, H_{app})\,dT \quad (3)$$

where the temperatures of the reservoirs, T_{hot} and T_{cold}, correspond to the extreme temperature ends of the full-width at half-maximum intensity (δT_{FWHM}) of the peak of the ΔS_{mag} *vs.* *T* curve.

3. Experimental results

3.1. Structural attributes

At room temperature, $(Fe_{47.5}Ni_{1.5})Rh_{51}$ is confirmed to adopt the chemically-ordered cubic B2 (CsCl)-type crystal structure with a calculated lattice parameter of $a_{FeRh\text{-}Ni} = 2.983$ Å ± 0.001 Å. The x-ray diffraction pattern, Fig. 1, indicates that the sample is crystallographically isotropic with a relatively high chemical order parameter $S = 0.81$. The widths of the XRD Bragg peaks are predominantly attributed to instrumental broadening and thus a high degree of crystallinity was assigned to this sample.

3.2. Effects of temperature and magnetic field on the magnetostructural transition

Temperature-dependent magnetization curves of $(Fe_{47.5}Ni_{1.5})Rh_{51}$ obtained at applied magnetic fields in the range $0\ T \le \mu_0 H_{appl} \le 3$ T in the absence of applied pressure (at $P = 0$ kbar) are shown in Fig. 2. At $\mu_0 H_{app} = 1$ T the sample exhibits a thermally-hysteretic AFM → FM magnetic phase transition at $T_t = 144$ K (thermal hysteresis width $\Delta T_t = 38$ K); a retained magnetization value denoted ΔM_{bkg} is observed for $T < T_t$ in the FC data. Application of increased magnetic field produces three simultaneous effects: i) an asymmetric shift in T_t to lower temperature values ($\left[\frac{\partial T_t}{\partial H}\right]_{AFM\to FM} = -19.1$ K/T and $\left[\frac{\partial T_t}{\partial H}\right]_{FM\to AFM} = -29.5$ K/T); ii) broadening of the magnetostructural transition width ΔT_t; and iii) an increase in the overall magnitude of the retained ferromagnetic signal ΔM_{bkg} for $T < T_t$. At an applied field of $\mu_0 H_{app} = 3$ T, the AFM → FM phase transition is no longer detected and complete stabilization of the ferromagnetic phase to lowest measured temperatures is observed.

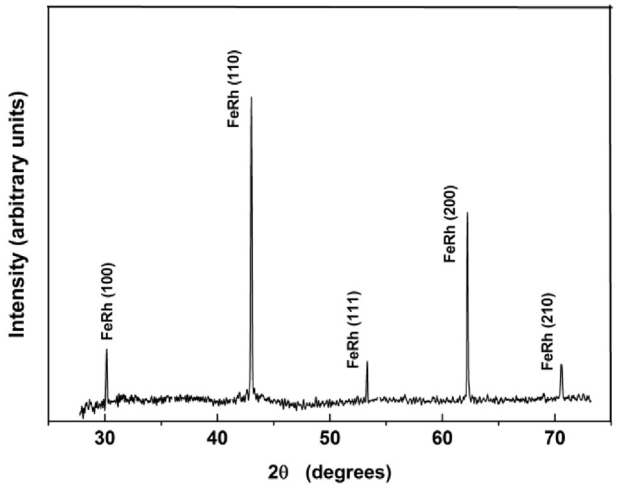

Fig. 1. X-ray diffraction pattern of the $(Fe_{47.5}Ni_{1.5})Rh_{51}$ compound. No crystalline phases other than the B2 (CsCl)-ordered crystal structure was observed in the annealed sample.

3.3. Effects of combined temperature, magnetic field and pressure on the magnetostructural transition

Field-cooled, temperature-dependent magnetization curves measured under the condition of simultaneous application of magnetic field ($\mu_0 H \le 5$ T) and of hydrostatic pressure ($P = 1.25$, 2.7, 5.4 and 8.1 kbar) are shown in Fig. 3. These data indicate that applied magnetic field and pressure influence the first-order magnetic transition in opposite ways. At a given applied magnetic field strength, increased applied pressure significantly increases T_t and decreases both ΔT_t and ΔM_{bkg}. Conversely, at a constant applied pressure, application of a magnetic field decreases T_t while concomitantly broadening ΔT_t and increasing ΔM_{bkg}. This compensating behavior allows the thermal hysteresis of the magnetic transition to be completely suppressed under an applied magnetic field $\mu_0 H = 4$ T with simultaneous applied pressure of $P = 1.25$ kbar, and at $\mu_0 H = 5$ T with simultaneous applied pressure of $P = 2.7$ kbar.

The experimental values of T_t^{cc}, T_t^{hc} and ΔT_t obtained at various applied pressure and magnetic field values are listed in Table 1; the transition temperatures of $(Fe_{47.5}Ni_{1.5})Rh_{51}$ as a function of applied pressure and of magnetic field, $T_t(P,H)$, are shown in Fig. 4. These data exhibit asymmetric linear trends corresponding to $(dT_t/dH)_{P=0} = -19.1$ K/T (at ambient pressure) and $(dT_t/dP)_{H=0} = 14.3$ K/kbar for the AFM → FM transition, and $(dT_t/dH)_{P=0} = -29.5$ K/T (at ambient pressure) and $(dT_t/dP)_{H=0} = 18.1$ K/kbar for the FM → AFM transition. The three-dimensional magnetic field–pressure–temperature ($\mu_0 H$–P–T) phase map determined for the first-order magnetic transition in the $(Fe_{47.5}Ni_{1.5})Rh_{51}$ system is shown in Fig. 5. The surface of the ($\mu_0 H$–P–T) diagram of Fig. 5 represents the isocompositional response of the magnetic transition temperature to combined application of pressure and magnetic field. The volume below the surface represents the stability range of the low-temperature antiferromagnetic (AF) state, while the space above the surface represents the stability range of the ferromagnetic (FM) state. The surface gradually drops to 0 K when the transition temperature is shifted to temperatures below ~100 K through application of magnetic field.

The calculated magnetic entropy curves (ΔS_{mag} *vs.* *T* plots) of the $(Fe_{47.5}Ni_{1.5})Rh_{51}$ sample at applied hydrostatic pressures ranging from 0 to 8.4 kbar and at an applied magnetic field of $H_{app} = 2$ T, are shown in Fig. 6(a). These curves were constructed from magnetization isotherms measured in the vicinity of the first-order magnetic transition. As an example, Fig. 6(b) shows magnetization isotherms of the sample at an applied pressure of 5.4 Kbar in the temperature range 223–251 K. At zero applied pressure, $(Fe_{47.5}Ni_{1.5})Rh_{51}$ demonstrates a table-like magnetic entropy curve with a shoulder at T = 132 K and a peak magnetic entropy change of $\Delta S_{mag}^{peak} = 6.2$ J/kgK at T = 160 K. Application of hydrostatic pressure increases ΔS_{mag}^{peak}, but decreases both the working temperature range (δT_{FWHM}) and the refrigeration capacity *RC*. The magnetocaloric properties of $(Fe_{47.5}Ni_{1.5})Rh_{51}$ determined from these data are summarized in Table 2.

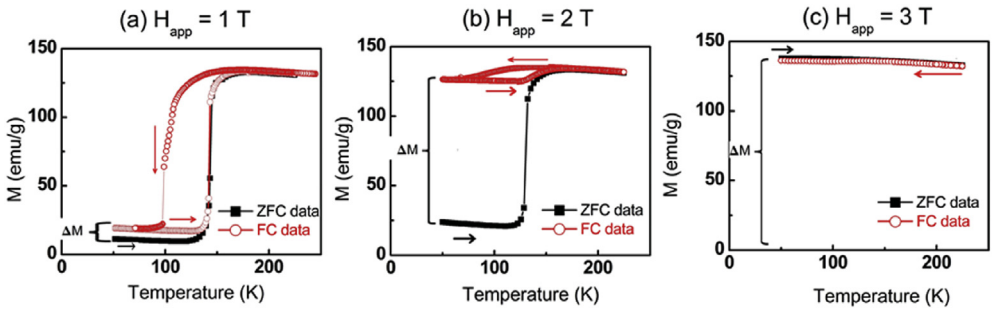

Fig. 2. Zero-field cooled (ZFC) and field-cooled (FC) temperature-dependent magnetic behavior of the $(Fe_{47.5}Ni_{1.5})Rh_{51}$ system at applied magnetic fields in the range $\mu_0 H_{app} = 1–3$ T and in the absence of pressure (P = 0 kbar).

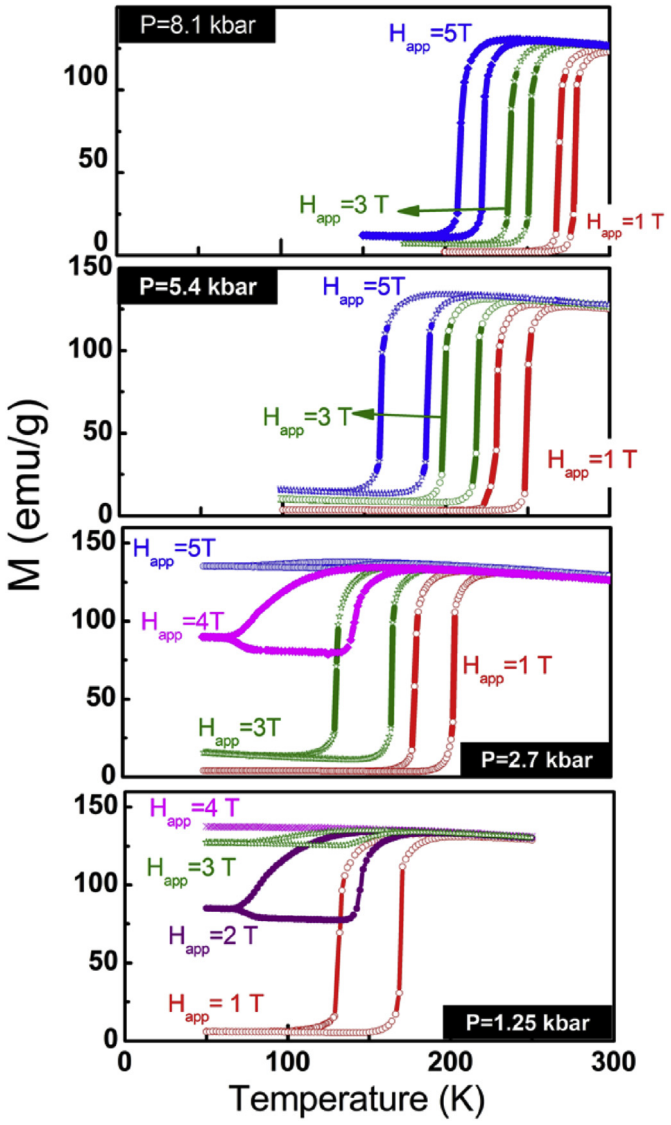

Fig. 3. Field-cooled temperature-dependent magnetization measurements under simultaneous application of magnetic field (up to 5 T) and hydrostatic pressure (up to 8.1 kbar).

4. Discussion

To better understand the influence of simultaneous application of temperature, pressure and magnetic field on the magnetostructural response of the $(Fe_{47.5}Ni_{1.5})Rh_{51}$ system, particular sections are devoted to three parameters: Section (i) addresses the first-order magnetic transition temperature (T_t); Section (ii) examines the thermal hysteresis width of the magnetic transition (ΔT_t); and Section (iii) describes the pressure and magnetic field dependence of the transition temperature ($(dT_t/dP)_{H=0}$ and $(dT_t/dH)_{P=0}$), respectively). Fundamental factors influencing pressure-induced magnetic entropy changes are discussed last, in Section (iv).

(i) First-order magnetic transition temperature

Consistent with previous reports [12–21] of the behavior of Ni-doped FeRh, the zero-field, zero-applied pressure first-order magnetic transition temperature $T_t|_{H=0,\Delta P=0} = 144$ K of $(Fe_{47.5}Ni_{1.5})Rh_{51}$ is found to occur at a significantly lower temperature than that of the parent FeRh compound, where $T_t|_{H=0,\Delta P=0} = 360$ K [12], shown in Fig. 3. At ambient pressure, the magnetic-field-induced decrease of the transition temperature $\partial T_t/\partial H|_{\Delta P=0} = -25$ K/T is accompanied by significant broadening of the thermal hysteresis width and by an increase in the magnetic background value (ΔM_{bkg}) in the low-temperature AFM regime. At the current time, ΔM_{bkg} is recognized as an experimental manifestation of the metastable retention of the high-temperature FM phase. Note that field-induced stabilization of the high-temperature FM phase is not observed in pure equiatomic bulk FeRh compounds [13–21]; prior to this study, such anomalous magnetothermal behavior in FeRh-based bulk compounds has only been noted in Pd-doped FeRh ternary systems of composition, $(Fe_{0.45}Rh_{0.45})Pd_{0.1}$ and $Fe_{0.49}(Rh_{0.93}Pd_{0.07})_{51}$ [25,29].

The origin of the unusual magnetic behavior of modified FeRh-based compounds of composition $(Fe_{47.5}Ni_{1.5})Rh_{51}$, $(Fe_{0.45}Rh_{0.45})Pd_{0.10}$ and $Fe_{0.49}(Rh_{0.93}Pd_{0.07})_{51}$ is partially attributed to valence electron concentration-induced changes to the electronic structure of the parent FeRh compound that shifts $T_t < 200$ K [30]. Magnetic field application further decreases T_t in these ternary FeRh systems and eventually the phase transformation dynamics becomes critically slow at low temperatures due to reduced ambient thermal energy. The magnetic response is inhibited completely in Ni- and Pd-doped FeRh compounds for T_t less than a critical value of ~75 K. It is thus construed that the magnetostructural phenomenon in FeRh-based compounds is a thermally-activated process. This hypothesis is consistent with the observation that no FeRh-ternary compound is reported to exhibit magnetostructural behavior for T < ~75 K (See Table 1 in the Supplementary Section of Reference 30 for a complete list of the T_t values of FeRh-ternary compounds). Similarly, kinetic arrest of the first-order magnetic transition response has also been reported in other magnetostructural systems such as in Cr-substituted Mn_2Sb alloys, Pr-substituted $La_{0.67}Ca_{0.33}MnO_3$ and $Nd_{0.5}Sr_{0.5}MnO_3$ [31–33].

Table 1
Experimental values of the magnetostructural transition temperatures of $(Fe_{47.5}Ni_{1.5})Rh_{51}$ at different applied hydrostatic pressures and magnetic fields.

P (kbar)	$\mu_0 H_{app}$ = 1 T		$\mu_0 H_{app}$ = 2 T		$\mu_0 H_{app}$ = 3 T		$\mu_0 H_{app}$ = 4 T		$\mu_0 H_{app}$ = 5 T	
	T_t^{hc} (K)	T_t^{cc} (K)	T_t^{hc} (K)	T_t^{cc} (K)	T_t^{hc} (K)	T_t^{cc} (K)	T_t^{hc}(K)	T_t^{cc} (K)	T_t^{hc} (K)	T_t^{cc} (K)
0	158	108	135	68	No magnetic transition		No magnetic transition		No magnetic transition	
1.25	169	137	144	87	134	65	No magnetic transition		No magnetic transition	
2.7	204	178	184	157	168	126	150	74	No magnetic transition	
5.4	247	234	232	217	217	200	202	180	187	159
8.1	294	284	280	270	266	256	252	242	238	228

*The transition temperatures, T_t^{hc} and were obtained upon heating through the AF → FM transition and cooling through the FM → AF transition respectively.

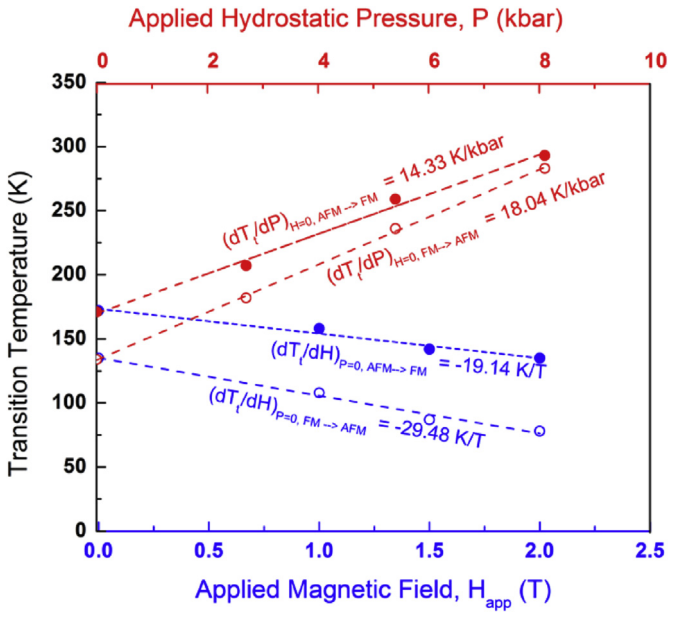

Fig. 4. Dependence of the transition temperatures of $(Fe_{47.5}Ni_{1.5})Rh_{51}$ system on hydrostatic pressure and (red symbols) and magnetic field (blue symbols). Open symbols and closed symbols represent transition temperatures obtained upon cooling and heating the sample, respectively. Dotted lines are linear fits to the data. (For interpretation of the references to colour in this figure legend, the reader is referred to the web version of this article.)

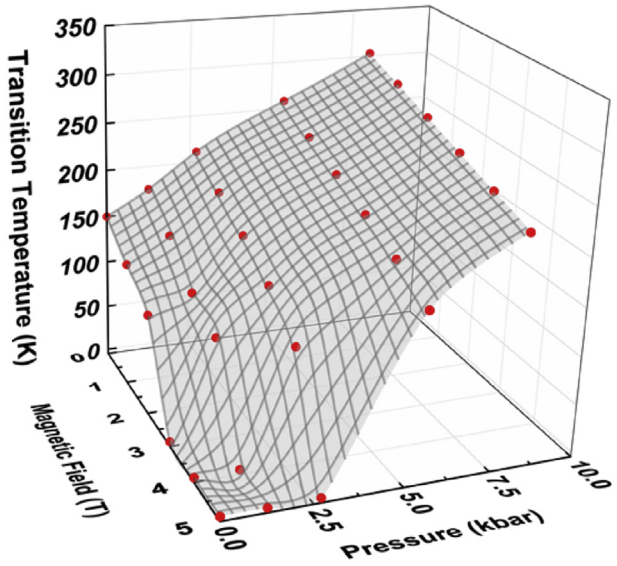

Fig. 5. Phase diagram derived from magnetic measurements in temperature, magnetic field and pressure space for $(Fe_{47.5}Ni_{1.5})Rh_{51}$ ($\mu_0 H < 5$ T, P < 10 kbar, T < 320 K). Dotted lines serve as a guide to the eye to highlight the sensitivity of the transition temperature to changes in magnetic field. Here, thermal hysteresis in the magnetostructural response was accounted for by utilizing the average transitions temperature obtained upon cooling through the FM → AF transition (T_t^{cc}) and heating through the AF → FM transition (T_t^{hc}) ($i.e. T_t = (T_t^{hc} + T_t^{cc})/2$) . The experimental values of T_t^{cc} and T_t^{hc} obtained at different applied pressure and magnetic fields are presented in Table 1.

(ii) Thermal hysteresis width

Characteristic of first-order phase transformations, thermal hysteresis of the magnetostructural phase transition is associated with kinetic barriers to nucleation of the lower-temperature phase. The experimental data obtained in this study indicate that the thermal hysteresis width (ΔT_t) of the $(Fe_{47.5}Ni_{1.5})Rh_{51}$ system increases with increasing magnetic field magnitude and decreases with increasing hydrostatic pressure (see Table 2). However, once the hysteresis width (ΔT_t) of $(Fe_{47.5}Ni_{1.5})Rh_{51}$ are plotted as a function of magnetostructural temperature (T_t), irrespective of pressure and magnetic field conditions, the data collapse into a universal curve as shown in Fig. 7. It is thus deduced that during magnetothermal cycling, nucleation and growth of the FM and the AFM phases in the $(Fe_{47.5}Ni_{1.5})Rh_{51}$ sample is influenced predominantly by temperature, not by application of pressure or of magnetic field. Therefore it is concluded that pressure and magnetic field have little influence on the specific activation energy barriers that a bulk FeRh system must overcome during the magnetostructural phase transformation process. The significant broadening of the magnetic transition width observed at low temperatures (see Figs. 2 and 3) is tentatively recognized as yet another experimental signature of the slow kinetics of the phase transformation process at low temperature due to low ambient thermal activation energy.

(iii) Pressure and magnetic field dependence of the magnetic transition temperature

It is well known that chemical modification of the FeRh lattice changes the pressure and field dependence of T_t relative to that of the equiatomic parent compound that exhibits values of $(dT_t/dP)_{FeRh} = 5.5$ K/bar at zero applied magnetic field [17,19] and $(dT_t/dH)_{FeRh} = 8.5$ K/T [12,21,25] at ambient pressure. The magnitudes of the trends of $(dT_t/dH)_{P=0}$ and $(dT_t/dP)_{H=0}$ of $(Fe_{47.5}Ni_{1.5})Rh_{51}$ are found in this work to be approximately three times greater than those of unmodified bulk FeRh ($(dT_t/dH)_{FeRh-Ni} = -14.2$ K/bar; $(dT_t/dP)_{FeRh-Ni} = 24.6$ K/T). The current data indicate that there is a significant difference in the values of the pressure and field dependences of T_t in $(Fe_{47.5}Ni_{1.5})Rh_{51}$ depending upon whether the transition occurs upon heating from the AFM → FM state ($(dT_t/dH)_{P=0} = -19.1$ K/T and $(dT_t/dP)_{H=0} = 14.3$ K/kbar) as compared to cooling from the FM → AFM state ($(dT_t/dH)_{P=0} = -29.5$ K/T and $(dT_t/dP)_{H=0} = 18.1$ K/kbar). This observation indicates that the

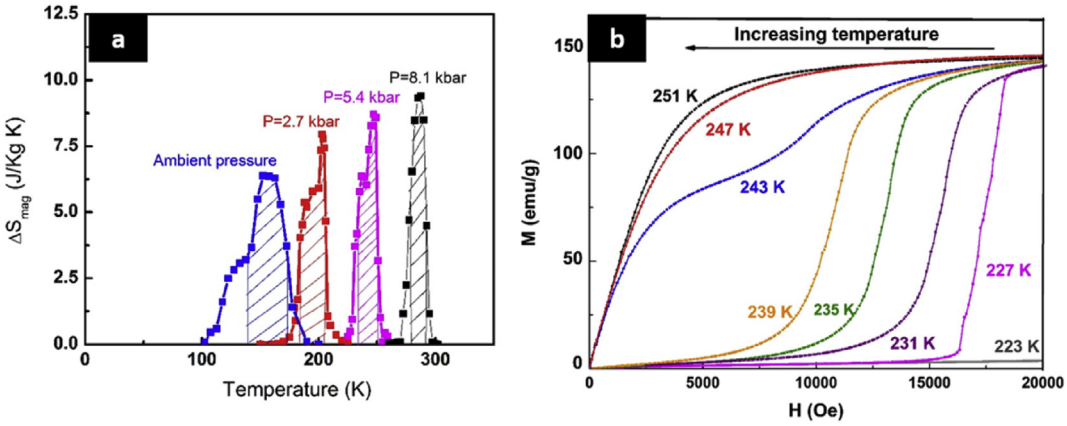

Fig. 6. (a) Magnetic entropy curves (ΔS_{mag} vs. T) of $(Fe_{47.5}Ni_{1.5})Rh_{51}$ system at an applied magnetic field of $H_{app} = 2$ T. The hatched area corresponds to the refrigeration capacity of the system at a given applied pressure. (b) Magnetization isotherms of $(Fe_{47.5}Ni_{1.5})Rh_{51}$ in a magnetic field of $H_{app} = 2$ T and hydrostatic pressure of 5.4 kbar in the temperature range 223–251 K.

Table 2
Experimental values of the magnetocaloric properties of $(Fe_{47.5}Ni_{1.5})Rh_{51}$ at different applied hydrostatic pressures and at an applied magnetic field of $\mu_0 H_{app} = 2$ T.

Pressure (kbar)	Magnetic entropy (J/kgK)	Refrigeration capacity (J/kg)	Working temperature range (K)		
			T_{hot}	T_{cold}	δT_{FWHM}
0	6.33	214	173	139	34
2.7	7.81	172	205	183	22
5.4	8.75	113.75	250	233	13
8.1	9.41	103.4	291	270	11

[a] The magnetocaloric properties reported in this table were measured at an applied magnetic field of $\mu_0 H_{app} = 2$ T.

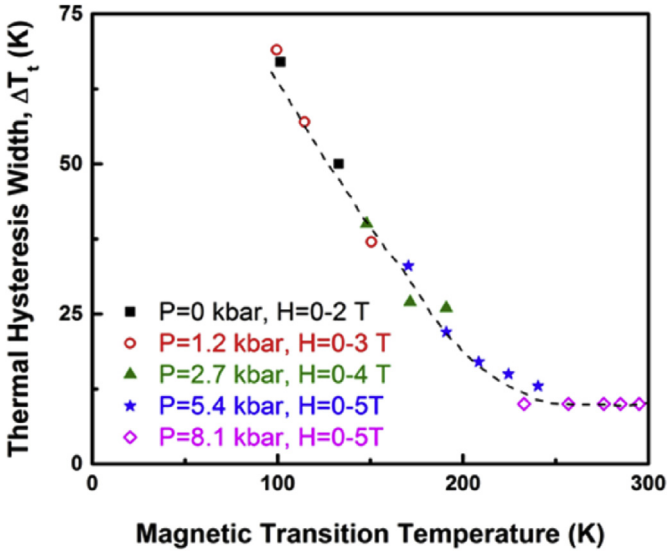

Fig. 7. Relationship between hysteresis width and the magnetostructural transition temperature of the $(Fe_{47.5}Ni_{1.5})Rh_{51}$ sample, as obtained under varying experimental pressure and magnetic field conditions. Dotted line serve as a guide to the eye.

barriers to nucleation of the equilibrium phase in this compound depend upon the initial magnetic state. Future work aimed at comparing the kinetic parameters (example: activation energy (E_a), isothermal time-dependence of the phase transformation, etc.) of the AFM → FM and FM → AF phase transformation in $(Fe_{47.5}Ni_{1.5})Rh_{51}$ would be useful in confirming this hypothesis. Prior to this present study, an asymmetry between the transition temperature sensitivity of the cooling and heating processes in B2-type FeRh-based systems transition has only been observed in Pd- and Au-doped FeRh bulk (4–8 at%) samples and in ultrathin (thickness < 20 nm) FeRh films grown epitaxially on MgO [30,33,34].

(iv) Magnetocaloric (MC) properties

From the perspective of use-inspired research, this study presents the first report of pressure-induced magnetic entropy changes in a doped FeRh-ternary compound. While the magnetic entropy change curves measured from many magnetostructural materials, including the parent FeRh compound, typically exhibit a sharp "caret"-shaped feature [8,16], the $(Fe_{47.5}Ni_{1.5})Rh_{51}$ compound demonstrates a flattened magnetic entropy change curve of "table-like" character. For potential commercial cooling applications involving the high-efficiency Ericsson cycle, a "table-like" MC response is necessary for regenerative balance and the achievement of high efficiency to approach that available from the Carnot cycle [8]. Broadening of the entropy curve increases δT_{FWHM} and despite significantly lower ΔS_{mag}^{peak} values, the $(Fe_{47.5}Ni_{1.5})Rh_{51}$ compound exhibits an enhanced net refrigeration capacity relative to that of the parent FeRh compound (RC_{FeRh} = 158 J/kg at $H_{app} = 2$ T [35,36]) by 35%. Based on the theoretical study of Imry and Wortis [37], it is proposed that broadening of the magnetic entropy change curve is partially attributed to the presence of microscopic randomly-sited Ni substitutional impurities in the FeRh lattice. Chemical disorder-induced broadening of the magnetostructural phase transition has also been reported in other magnetocaloric materials systems such as $Gd_5Ge_2Si_{x-2}Fe_x$ and alloys of $CoMnGe_{1-x}Sn_x$ [8]. At the current time, the underlying mechanism for the observed decrease in the "table-like" character of the magnetic entropy curve with increase in hydrostatic pressure is not clearly understood (see Fig. 6) and is likely correlated with

the lethargic phase transition kinetics existing at low temperatures. Once the $(Fe_{47.5}Ni_{1.5})Rh_{51}$ transition is shifted to high temperatures by application of hydrostatic pressure, the thermal energy required to drive the phase transformation decreases and thus the sharpness of the magnetic entropy curve is eventually restored.

5. Conclusions

In this work, $(Fe_{47.5}Ni_{1.5})Rh_{51}$ serves as a model system for understanding the relative and simultaneous effects of temperature (2 K – 400 K), magnetic field (up to 5 T) and pressure (up to 10 kbar) on the magnetostructural response of FeRh-based systems. The experimental data and trends presented in this work indicate that external pressure and magnetic field influence the magnetostructural properties of FeRh-based compounds in opposite ways (T_t increases with increasing pressure and decreases with increasing magnetic field; conversely, the transition width ΔT_t decreases with increasing pressure and increasing magnetic field). It is proposed that when the $(Fe_{47.5}Ni_{1.5})Rh_{51}$ transition is shifted to low temperatures ($T < 200$ K), first by elemental substitution and then by application of a magnetic field, the magnetostructural transition process becomes arrested in metastable regimes due to low thermal activation energy. Consequently, at low temperatures, significant broadening of the magnetic transition width is accompanied by an anomalous increase in the sensitivity of the magnetostructural temperature to pressure and magnetic field. At a critical temperature of ~75 K, complete suppression of the $(Fe_{47.5}Ni_{1.5})Rh_{51}$ phase transformation process is observed. Examination of the magnetocaloric properties of $(Fe_{47.5}Ni_{1.5})Rh_{51}$ at an applied magnetic field of 2 T reveals that pressure increases the magnetic entropy (ΔS_{mag}), while decreasing the refrigeration capacity (RC) and the working temperature range (δT_{FWHM}) of the sample. Overall, these results emphasize that the magnetostructural phenomena in FeRh-based compounds is a thermally-activated process that may be tuned predictably by a variety of intrinsic (elemental substitution) or extrinsic (pressure, magnetic field, temperature) factors.

Acknowledgements

Research was performed under the auspices of the U.S. Department of Energy, Division of Materials Science, Office of Basic Energy Sciences under Contract No. DE-SC0005250 [R.B., I.M, F.J.V., and L.H.L.] and the National Science Foundation under Grant No. ECCS-1402738[D.H.]

References

[1] D.A. Filippov, R.Z. Levitin, A.N. Vasil'ev, T.N. Voloshok, H. Kageyama, R. Suryanarayanan, Phys.Rev. B 65 (2002), 100404.
[2] L. Morellon, J. Stankiewicz, B. Garc, A. Landa, P.A. Algarabel, M.R. Ibarra, Appl. Phys. Lett. 73 (1998) 3462–3464.
[3] E. Stern-Taulats, A. Planes, P. Lloveras, M. Barrio, J.-L. Tamarit, S. Pramanick, S. Majumdar, C. Frontera, L. Mañosa, Phys. Rev. B 89 (2014), 214105.
[4] S.A. Nikitin, G. Myalikgulyev, M.P. Annaorazov, A.L. Tyurin, R.W. Myndyev, S.A. Akopyan, Phys. Lett. A 171 (1992) 234–236.
[5] V.K. Pecharsky, K.A. Gschneidner, Phys. Rev. Lett. 78 (1997) 4494–4497.
[6] S.A. Nikitin, G. Myalikgulyev, A.M. Tishin, M.P. Annaorazov, K.A. Asatryan, A.L. Tyurin, Phys. Lett. A 148 (1990) 363–366.
[7] N. Sarawate, M. Dapino, Appl. Phys. Lett. 88 (2006), 121923.
[8] K.A. Gschneidner, V.K. Pecharsky, Annu. Rev. Mater. Sci. 30 (2000) 387–429.
[9] I. Karaman, B. Basaran, H.E. Karaca, A.I. Karsilayan, Y.I. Chumlyakov, Appl. Phys. Lett. 90 (2007), 172505.
[10] C.J. Sun, D.B. Xu, D.L. Brewe, J.S. Chen, S.M. Heald, G.M. Chow, Magn. IEEE Trans. Mag. 49 (2013) 2510–2513.
[11] X. Marti, I. Fina, C. Frontera, J. Liu, P. Wadley, Q. He, R.J. Paull, J.D. Clarkson, J. Kudrnovský, I. Turek, J. Kuneš, D. Yi, J.H. Chu, C.T. Nelson, L. You, E. Arenholz, S. Salahuddin, J. Fontcuberta, T. Jungwirth, R. Ramesh, Nat. Mater. 13 (2014) 367–374.
[12] J.S. Kouvel, C.C. Hartelius, J. Appl. Phys. 33 (1962) 1343.
[13] F.D. Bergevin, L. Muldawer, CR. Acad. Sci. 252 (1961) 1347.
[14] J.S. Kouvel, J. Appl. Phys. 37 (1966) 1257.
[15] D.W. Cooke, F. Hellman, C. Baldasseroni, C. Bordel, S. Moyerman, E.E. Fullerton, Phys. Rev. Lett. 109 (2012), 255901.
[16] M.P. Annaorazov, S.A. Nikitin, A.L. Tyurin, K.A. Asatryan, A.K. Dovletov, J. Appl. Phys. 79 (1996) 1689.
[17] R.C. Wayne, Phys. Rev. 170 (1968) 523.
[18] A.I. Zakharov, A.M. Kadomtseva, R.Z. Levitin, E.G. Ponyatovskii, Sov. Phys. JETP 19 (1964) 1348.
[19] L.I. Vinokurova, A.V. Vlasov, M. Pardavi-Horváth, Phys. Stat. Sol. B 78 (1976) 353.
[20] K. Kamenev, Z. Arnold, J. Kamarád, N.V. Baranov, J. Appl. Phys. 81 (1997).
[21] I. Suzuki, T. Koike, M. Itoh, T. Taniyama, T. Sato, J. Appl. Phys. 105 (2009).
[22] R. Barua, X. Jiang, F. Jimenez-Villacorta, J.E. Shield, D. Heiman, L.H. Lewis, J. Appl. Phys. 113 (2013), 023910.
[23] R. Barua, F. Jimenez-Villacorta, J. Shield, D. Heiman, L. Lewis, J. Appl. Phys. 113 (2013), 17B523.
[24] P. Kushwaha, A. Lakhani, R. Rawat, P. Chaddah, Phys. Rev. B 80 (2009), 174413.
[25] P. Kushwaha, R. Rawat, P. Chaddah, Appl. Phys. Lett. 106 (2) (2015), 022404.
[26] G.A. Novak, A.A. Colville, Am. Mineral. 74 (1989) 488–490.
[27] EasyLab Mcell 10 – 10 kbar hydrostatic pressure cell for Quantum Design MPMS measurement platform, Technical Motes from Almax EasyLab.
[28] M. Manekar, S.B. Roy, J. Phys. D. Appl. Phys. 41 (2008), 192004.
[29] Y. Feng, T. Fukuda, T. Kakeshita, J. Alloys Compd. 577 (Suppl. 1) (2013) S52–S55.
[30] R. Barua, F. Jimenez-Villacorta, L. Lewis, Appl. Phys. Lett. 103 (2013), 102407.
[31] P. Kushwaha, P. Bag, R. Rawat, P. Chaddah, J. Phys. Cond. Mat. 24 (9) (2012), 096005.
[32] R. Rawat, K. Mukherjee, K. Kumar, A. Banerjee, P. Chaddah, J. Phys. Condens. Mat. 19 (2007), 256211. J. Phys. Cond. Mat. 20.
[33] M.K. Chattopadhyay, S.B. Roy, A.K. Nigam, K.J.S. Sokhey, P. Chaddah, Phys. Rev. B 68 (2003), 174404.
[34] M. Loving, M.A. de Vries, F. Jimenez-Villacorta, C.H. Marrows, L.H. Lewis, J. Appl. Phys. 112 (4) (2012), 043512.
[35] C.J. Kinane, M. Loving, M.A. de Vries, R. Fan, T.R. Charlton, J.S. Claydon, D.A. Arena, F. Maccherozzi, S.S. Dhesi, D. Heiman, C.H. Marrows, L.H. Lewis, Sean Langridge, New. J. Phys. 16 (2014), 113073.
[36] R. Barua, F. Jimenez-Villacorta, L. Lewis, J. Appl. Phys. 115 (2014), 17A903.
[37] Y. Imry, M. Wortis, Phys. Rev. B 19 (7) (1979), 3580.